Materials & Design 212 (2021) 110269

Contents lists available at ScienceDirect

Materials & Design

journal homepage: www.elsevier.com/locate/matdes

Temperature rise up to melting under quasi-static loading conditions induced by adiabatic shear banding

L. Choisez, G. Roy, P.J. Jacques *

UCLouvain, Institute of Mechanics, Materials and Civil Engineering, IMAP, Place Sainte Barbe, 2, B-1348 Louvain-la-Neuve, Belgium

HIGHLIGHTS

- Use of the fusible coating method with several coatings instead of one until now.
- Comparison of two 1-D heat diffusion equations based on experimental measurements.
- Physically-based 2-D heat diffusion model, with experimentally confirmed predictions.
- Equations predicting the maximum temperature rise during adiabatic shear banding.

GRAPHICAL ABSTRACT

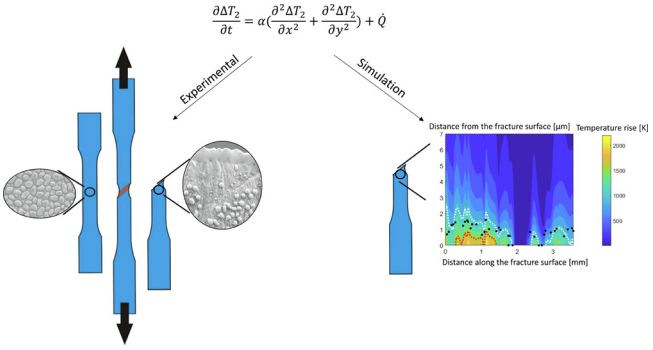

ARTICLE INFO

Article history:
Received 7 August 2021
Revised 30 October 2021
Accepted 21 November 2021
Available online 22 November 2021

Keywords:
Adiabatic shear banding
Temperature rise
Fusible coating method
Two-dimensional heat diffusion model
Metastable Ti alloy

ABSTRACT

Adiabatic shear banding propagating at very large speed was observed during the unstable fracture of TRIP-TWIP β -metastable Ti-12 wt% Mo alloy under quasi-static loading. The fusible coating method was used with five different coatings to assess the predicted temperature variations. Two one-dimensional models are compared based on parameters measured on fractured samples of Ti-12 wt% Mo alloy. The importance of the thickness of the shear band as well as of the shearing time are highlighted. A new two-dimensional model is then developed to represent the nucleation and propagation of the shear band. Finally, an analytical one-dimensional model is proposed to estimate the temperature rise occurring during adiabatic shear banding of other metallic alloys from easily accessible physical and mechanical properties.

1. Introduction

Adiabatic shear banding (ASB) was recently identified during the fracture of TRIP-TWIP β -metastable Ti-12 wt% Mo alloy under quasi-static loading [1,2]. Adiabatic shear banding occurs when the strains localize in a shear band with a very large associated strain rate. It can be activated when softening mechanisms, including thermal softening, significantly overcome the different work hardening sources. Thermal softening occurs when the heat production rate is larger than the heat dissipation rate, i.e. usually during dynamic loading. Hence, adiabatic shear banding was mainly studied during controlled dynamic testing [3], but it has also been observed at quasi-static strain rate at very low temperatures [4], or in materials with very low work hardening such as nanocrystalline materials or bulk metallic glasses [5,6]. The investigated Ti-12 wt% Mo alloy, called Ti-12Mo hereafter, does not fit with these criteria as it presents a very large work hardening [7] while it was loaded at quasi-static strain rate at room temperature.

The activation of adiabatic shear banding was related to a very large crack propagation speed in Ti-12Mo [2]. Because of its very large ductility as well as its damage resistance [1], plastic deforma-

* Corresponding author.
E-mail address: pascal.jacques@uclouvain.be (P.J. Jacques).

https://doi.org/10.1016/j.matdes.2021.110269
0264-1275/

tion strongly localizes in a shear band at the end of plastic deformation of flat tensile samples in which fracture eventually initiates [2]. While the maximum speed of a shear band generally increases linearly with the loading speed [8–11], simulations predict a saturation of the shear band propagation speed for very large loading speeds [12,13]. According to Bonnet-Lebouvier *et al.* [13], two stages can be distinguished depending on the loading speed: a first stable stage in which the shear band propagation speed is governed by the external work; and a second unstable stage in which the shear band propagation speed becomes independent on the external work and sensitive to the inertial effects. The theoretical maximum speed of a shear band in its unstable regime was estimated around 50–60% of the elastic shear wave speed [12,14,15]. In the case of Ti-12Mo, the crack propagation speed increases up to 1840 $m\,s^{-1}$, i.e. approximately 59% of the speed of a shear wave in this material, corresponding to a shear band propagating in an unstable regime [2].

A significant temperature rise occurring during the fracture was confirmed by the use of the fusible coating method with Sn and Cu coatings [1,2]. Large temperature rise associated with adiabatic shear banding during quasi-static loading is not restricted to Ti-12Mo alloy. Makel *et al.* [8–10] observed the formation of adiabatic shear banding as well as melted patterns on the fracture surfaces during the strain localization in shear lips and unstable fracture of several Ti alloys (Ti-6Al-4V, Ti-8Mn, Ti-10V-2Fe-3Al) and of a 4340 steel during quasi-static loading. Adiabatic shear banding can be at the origin of many microstructural changes. Indeed, a local dynamic recrystallization was observed in Ti-12Mo [1]. An accurate estimation of the local temperature rise is therefore needed to understand these local transformations.

Temperature rise during ASB propagation has been analyzed either based on analytical solutions [11,12] or on mesh or meshless finite element (FE) simulations [13–18]. FE simulations allow a thermomechanical coupling at each step of the deformation, as well as the estimation of the local stresses, strains, strain rates and temperatures during the band propagation. However, such models can be heavy to implement, time consuming and requiring the complete evolution of the material flow stress with strain, strain rate and temperature as input data, as well as sometimes a critical strain/temperature at which the constitutive model has to be changed to represent additional softening mechanisms caused by damage and/or local transformation into a viscous fluid.

Different authors tried to measure experimentally the temperature rise occurring during adiabatic shear banding using an array of high-speed infrared detectors, but the temporal resolution was limited (~0.5 μs) and the spot size of these detectors (5.5–100 μm) was generally larger than the width of the shear bands [19–25]. It is also worth noting that experimentally studied adiabatic shear bands generally correspond to the "stable" phase of ASB propagation, for which the shear band propagation speed is controlled by the loading speed [25]. ASB propagation during fracture of Ti-12Mo corresponds to the "unstable" phase of ASB propagation [25], where the shear band propagation speed saturates at a maximum value bounded by the speed of an elastic shear wave [2]. As a consequence, the shearing time is very short (~0.2 μs). Moreover, the thickness of the ASB formed in Ti-12Mo is very small, in the range of 1–3 μm [1]. Excellent temporal and spatial resolutions are therefore needed to measure the temperature rise occurring during the fracture of Ti-12Mo.

The use of the fusible coating method allows an indirect estimation of the maximum temperature rise reached in and close to the band, with excellent spatial and temporal resolutions. The fusible coating method was proposed by Lewandowski and Greer [26] to estimate the heat content and the maximum temperature reached in a shear band during the fracture of a bulk metallic glass. It consisted originally in a thin film of Sn coated on the surface of a bend-test specimen before loading. After fracture, the length over which the coating melted was correlated to the heat content produced in the shear band with a simple one-dimensional heat diffusion equation. This heat content was however overestimated by Lewandowski and Greer [26] as the heat production was considered as instantaneously produced in a plane. Battezatti *et al.* [27] considered the production of heat at a given rate in a shear band with a given thickness and shearing time by finite element simulation. However, they underestimated the shearing time by taking the speed of an elastic shear wave as the shearing speed. It was argued by Georgarakis *et al.* [28] and Miracle *et al.* [29] that the shearing speed is bounded by the time of redistribution of elastic stresses at the tip of the propagating shear band, corresponding to a shearing speed of about 10% of the speed of an elastic shear wave. Georgarakis *et al.* [28] and Slaughter *et al.* [30] highlighted the importance of a short shearing time to allow sufficient temperature rise, but they did not take into account the thickness of the shear band. Wang *et al.* [31] proposed an analytical model taking into account both the thickness and shearing time, showing the superior influence of the shearing time compared to the influence of the thickness. Different estimates were given for the shearing time in the literature, either measured by high speed imaging techniques [21,23,32] or estimated from a fraction of the speed of a transverse sound wave [15,16,19,25,26,29,33].

In these different models, ASB propagation is considered quasi-instantaneous, homogeneous through the section of the specimen and therefore translated as one-dimensional heat diffusion equation. However, ASB is a physical mechanism comprising a nucleation and a propagation stage [19,34]. Furthermore, the ASB propagation speed is not constant during unstable fracture, particularly in the case of Ti-12Mo [2]. A two-dimensional heat diffusion equation is thus mandatory to model the temperature rise during ASB propagation. Miracle *et al.* [29] proposed a pseudo 2D-heat diffusion equation by replacing the time dimension by a second space dimension with the use of the shear band propagation speed in a 1D-film heat diffusion equation. They considered that the entire heat content is released at the nucleation spot and then diffused and traveled in the shear band with the crack propagation. However, the local temperatures cannot be considered to move at the same speed as the ASB propagation so that this pseudo-2D heat diffusion equation is physically incorrect.

In this work, the shearing time was estimated from the evolution of the fracture speed measured by high speed imaging [2]. The fusible coating method was used with five different coatings to measure the maximum temperature rise reached at different distances from the fracture surface. The experimental reconstituted curve of the maximum temperature rise reached with respect to the distance to the center of the shear band was then used to compare two one-dimensional models: (i) the model originally proposed by Lewandowski *et al.* [26] considering an instantaneous heat produced in a plane and (ii) the heat diffusion equation with the heat produced homogeneously in a shear band of finite thickness during a finite time, as proposed by Wang *et al.* [31]. Furthermore, a new two-dimensional finite element model was developed by extending the one proposed by Wang *et al.* [31] to present the evolution of the temperature during the complete ASB propagation. Eventually, a set of simple analytical equations will be proposed to estimate the temperature rise that would occur in other alloys during a hypothetical unstable fracture based on easily accessible mechanical and physical properties.

2. Materials and methods

Ingot of Ti-12Mo alloy was processed from commercially pure titanium and molybdenum by the self-consumable melting tech-

nique. The chemical composition after casting, measured by Inductively Coupled Plasma (ICP), gave Ti-11.8Mo-0.02Fe-0.01Cu-0.0115O (in wt.%). A 10 mm-thick slice of the ingot was β - solutionised at 900 °C during 15 min, followed by water quenching. It was then cold rolled down to 1.0 mm, corresponding to a reduction level of 90%. A recrystallization treatment was carried out at 900 °C for 15 min in high-purity Ar atmosphere, followed by water quenching to retain the fully β microstructure at room temperature. It is worth noting that nano-sized athermal ω_{ath} phase is also present in the microstructure, as shown in previous work [7].

Uniaxial tension was carried out on specimens with a calibrated gauge length of 26 mm, and a gauge section of 1.1 × 6.1 mm^2 at 1 mm min^{-1}. They were previously polished down to 1 μm diamond paste and OPS. Prior to tensile testing, five different coatings were deposited on the tensile specimen, with increasing melting temperature: Sn ($T_m = 232$ °C), Zn ($T_m = 419.5$ °C), Al ($T_m = 660$ °C), Cu ($T_m = 1085$ °C) and Pd ($T_m = 1555$ °C). The coatings were deposited by PVD at a speed of 2 Å s^{-1} for Sn and 1 Å s^{-1} for the other coatings.

The area of the fracture surface was estimated as the product of the smallest width and the smallest thickness in the most deformed part of the tensile specimen. The thickness was averaged on 10 measurements through the width. The true tensile fracture stress and strain were calculated from the area of the fracture surface, as the mean (± standard deviation) of the true tensile fracture stress and strain of each coated tensile specimen. The angle formed by the fracture surface was measured by White Light Interferometry.

The specific heat capacity was measured by differential scanning calorimetry under Ar atmosphere, at a rate of 10 K min^{-1} from room temperature to 1273 K. The thermal diffusivity was measured by the laser flash technique, in agreement with the ASTM E-1461 standard. The thermal diffusivity was averaged from three measurements estimated at 300, 873, 1073, 1273, 1373, 1473, 1573 K, with a plateau of 50 min before the first heat shot and a heat rate of 10 K min^{-1} between each temperature. The evolution of the density was measured by dilatometry under vacuum, at a heating/cooling rate of 1 °C s^{-1}, with a plateau of 60 s at the maximum temperature (1223 K).

It is worth noting that the determination of the thermophysical properties of Ti-12Mo suffers from some uncertainties related to the metastable state of the microstructure which is mechanically tested, with respect to the more thermodynamically stable state on which these physical properties were estimated. However, it can be postulated that the measured values are representative of the investigated alloy. The details of the evolution of the specific heat capacity, thermal diffusivity and density of Ti-12Mo with temperature are given in Supplementary Figs. 1, 2 and 3.

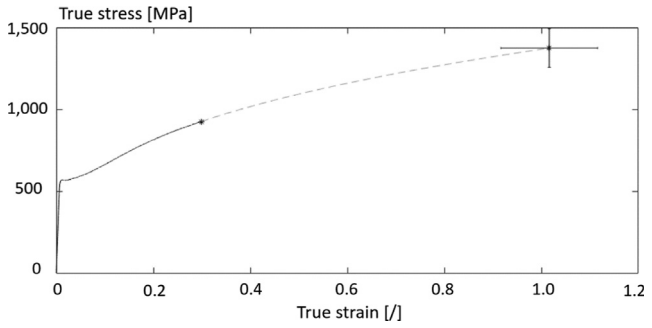

Fig. 1. True stress – true strain curve of the investigated Ti-12Mo alloy. The post-necking curve is extrapolated up to the true fracture strain and stress, averaged on 5 measurements and drawn with their standard deviations.

3. Results

3.1. Mechanical properties

Fig. 1 presents the true stress - true strain curve of Ti-12Mo. The post-necking behavior is an extrapolated power-law fit between the necking point and the true tensile fracture point. A true tensile fracture stress of 1375 ± 118 MPa was estimated from the last recorded force and fracture area of the five coated tensile specimens. Its large strain-hardening brings a large ductility in terms of true uniform strain (0.3) but also in terms of true tensile fracture strain (1.02 ±0.10).

3.2. Fusible coating method

Fig. 2 presents the morphology of the coatings in the as deposited state before tensile testing as well as after tensile testing. The

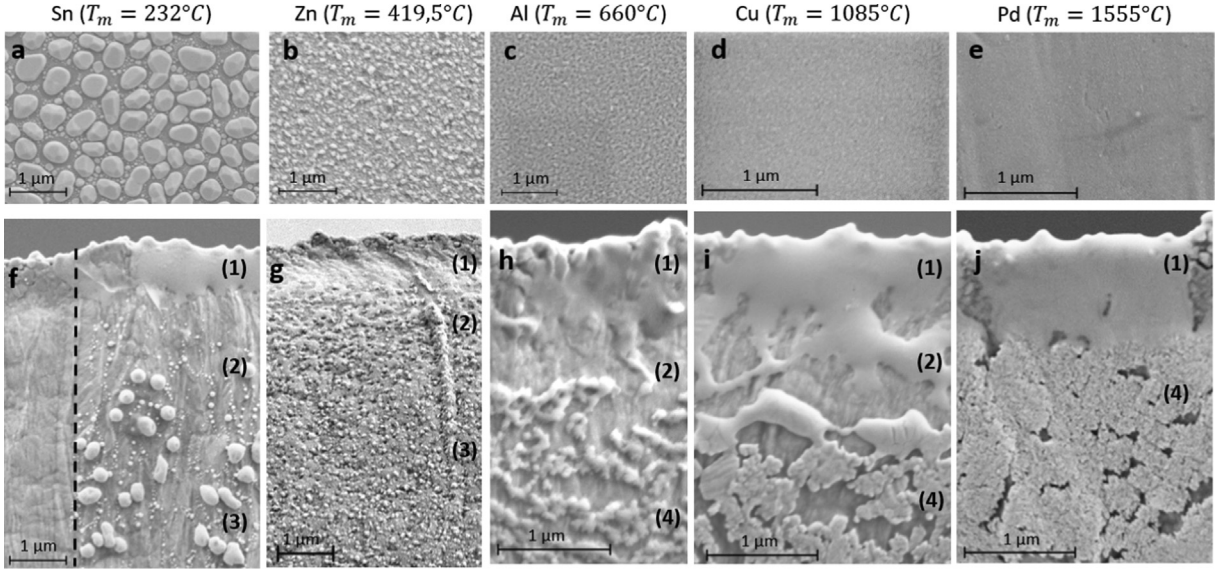

Fig. 2. SEM micrographs of the coatings before (a-e) and after the tensile test (f-j) near the fracture surface, presented in increasing order of their melted temperatures T_m: Sn (a-f), Zn (b-g), Al (c-h), Cu (d-i), Pd (e-j). 4 zones can be distinguished in the coating morphology after the tensile test: the coating (1) melted and resolidified continuously; (2) melted and resolidified discontinuously; (3) partially melted; (4) did not melt. (f) A line of Sn coating parallel to the tensile direction was removed before the test. The frontier between the coated and non-coated part of the tensile specimen is highlighted by the black dashed line.

initial coating (Fig. 2(a)-(e)) is continuous in the case of Al, Cu and Pd but non-continuous in the case of Sn and Zn. After fracture (Fig. 2(f)-(g)), the morphology of the coatings near the fracture surface is modified. Every coating melted close to the fracture surface, proving that the temperature reached at least 1828 K there. Different zones can be distinguished, even though they are not present on every specimen; a first zone (1) where the coating melted and resolidified as a continuous layer; a second zone (2) where the coating melted and resolidified discontinuously; a third zone (3) where some coatings partially melted; and a fourth zone (4) where the coating did not melt but were deformed by the tensile elongation. Fig. 2(f) illustrates the appearance of a non-coated part of the tensile specimen (on the left of the dashed line). Zone (1) corresponds to a specific part of the fractured tensile specimen where the material is the most deformed, closer to the fracture surface.

For the coatings with the lowest melting temperature (Sn and Zn coatings), the transition between the melted coating and non-melted coating is not clear and a zone (3) with partially melted coating appears. It is considered that the melting temperature was reached at the limit between the partially melted zone (3) and non-melted zone (4). Fig. 2(h) presents the case of Al coating. Apart from zone (1) where the coating is continuous, it is difficult to differentiate the non-melted coating from the melted coating underneath as the surface roughness of the coating is not modified by its melting. The transition between melted and non-melted coating length was set based on the larger wettability of the coating near the fracture zone. Fig. 2(i) presents the case of Cu coating. The transition between the melted coating (2) and the non-melted coating (4) is very clear. Fig. 2(j) presents the case of Pd coating, which always melted along the whole zone (1), corresponding to the specific deformation level in the material (see non-coated part of Fig. 2(f)). Its melted length corresponds therefore to the length of zone (1).

In order to use the fusible coating method, the distance at which the coating melted must be taken at the shortest distance from the fracture surface, i.e. perpendicularly and not along the coated side as they were measured. The smallest distance to the fracture surface is given by $x = l.\cos\theta$ [26], where l is the length of melted coating measured along the coated side and θ is the associated angle formed between the fracture surface and the horizontal direction (i.e. perpendicularly to the tensile direction). Table 1 presents the average angle θ (mean $\pm$ standard deviation), measured melted length l and the associated distances x for the five coatings.

4. Discussion

4.1. Fracture scenario

The heat diffusion models presented in the next sections were adapted to the fracture process of Ti-12Mo that can be summarized as follows. Ti-12Mo presents a very large ductility, leading to diffuse then localized necking with hardly any damage occurrence [2]. At a true strain level around 1.0, a crack initiates at the surface of the tensile specimen in the necking zone by a pure mode III shear, i.e. the material is sheared through its thickness but the crack propagates towards the direction of its width. A thin shear band is formed and equiaxed cavities are formed in the center of the tensile specimen inside the shear band, changing the pure mode III fracture into a mixed mode I-III fracture in the center of the specimen. At the end of the crack propagation, mode III fracture evolves into a mode II fracture at the edges of the specimen, with the material sheared through its width (i.e. with the shear direction parallel to the crack propagation direction) [2].

For each coated specimen, the coating melted only on one of the two fractured parts near the fracture surface, proving that a non-negligible temperature rise occurs only after the fracture initiation [2]. Moreover, the wettability of the melted coating present on the fracture surface increases when moving closer to the center of the fracture surface, proving that the local temperature increases during the shear event through the thickness of the tensile specimen [2]. Therefore, a large heat release rate at the origin of the non-negligible temperature rise is produced during the mode III shearing process.

Finally, a large variation in the length of melted coatings was measured along the fracture surface, showing that the temperature rise is not constant but varies during the crack propagation [2]. Some melted patterns were also found on the fracture surface and were associated with the location of the largest lengths of melted coatings [2], proving that a local temperature close to the melting temperature of the alloy is reached during its fracture.

4.2. Advantages and disadvantages of the different coatings

Five different coatings were considered to characterize the temperature rise occurring during the fracture of Ti-12Mo. Not all of them were perfectly suited as the limit between the melted and non-melted zones are sometimes difficult to set. Aluminum for example does not seem to fit correctly the fusible coating method in this case because the melted and resolidified Al coating mostly kept the same appearance as the non-melted coating, leading to a quasi-systematic underestimation of the limit between the non-melted and the melted coating.

Choosing a coating with a low melting temperature results in larger variations of the length of melted coatings with the variation of the local temperature, hence allowing a better sensitivity to variations of the heat release rate. However, coatings with a low melting temperature such as Sn ($T_m = 505$ K) and Zn ($T_m = 692.5$ K) gave rise to a zone with partially melted coating (see Fig. 2(f)-(g)), decreasing the accuracy of the measurements. When the melting temperature of the coating is very close to the maximum temperature reached as for the Pd coating ($T_m = 1828$ K) in the case of Ti-12Mo, a low sensitivity to the temperature variation is obtained, as the Pd coating always melted on a distance smaller than 1 μm, along the whole length of zone (1) (see Fig. 2(j)). However, choosing coatings with a melting temperature close to the maximum temperature reached, such as Cu ($T_m = 1358$ K) or Pd in the case of Ti-12Mo, allow a high accuracy of the fusible coating method measurement, with a clear transition between the melted and resolidified coating and the non-melted coating.

Table 1
Length of melted coating l [μm] measured on the fractured tensile specimen and the corrected minimum distance from the fracture surface × [μm] for each coating.

Coating	Sn	Zn	Al	Cu	Pd
T_m [K]	505	692.5	933	1358	1828
θ [°]	42 ± 7	41 ± 4	37 ± 6	43 ± 5	38 ± 7
l [μm]	8.0 ± 3.8	5.8 ± 3.9	1.1 ± 0.7	1.0 ± 0.6	0.8 ± 0.2
x [μm]	5.8 ± 2.7	4.3 ± 2.8	0.9 ± 0.6	0.8 ± 0.5	0.6 ± 0.1

4.3. Parameters of the models

Three models estimating the temperature rise in the shear band are considered here, with increasing accuracy as well as computation time. All three models are built around a common set of parameters that will be first assessed. The parameters are divided between the thermo-physical properties of the alloy (density, heat capacity, thermal diffusivity, Taylor-Quinney coefficient), the geometry of the shear band measured on fractured tensile specimens (thickness of the band, length of the shear offset) and the mechanical parameters (average true shear stress at fracture, shearing speed). The parameters used are summarized in Table 2.

The thermo-physical properties of the alloy, i.e. density ρ, heat capacity C_p and thermal diffusivity α, vary with temperature (Supplementary Figs. 1, 2 and 3). However, some models consider fixed values of these physical properties. The question thus arises of the temperature at which the physical properties have to be considered. In the present case, this temperature was chosen by comparing the calculated temperature distribution (detailed in Section 4.5) using fixed values with the results based on the physical properties varying with temperature. The best correspondence was obtained using the physical properties of Ti-12Mo at 1118.5 K (Supplementary Fig. 4).

Regarding the geometrical characteristics of the shear band, the half thickness of the shear band h was deduced from the observation of the fractured tensile specimen with and without coating shown in Fig. 2(f). We propose that the zone called zone (1) in Fig. 2(f) corresponds to the half-thickness of the shear band. Indeed, this zone is thinner than the rest of the fractured specimens and presents the highest wettability for the different coatings, i.e. a significantly larger temperature was always reached in this zone (at least 1828 K according to the melting of the Pd coating). The length of zone (1) was measured as $l = 0.7 \pm 0.1$ μm for every fractured tensile specimens. However, the half-thickness of the shear band h must be taken perpendicularly to the fracture surface as for the coating melted lengths: $h = 0.5 \pm 0.1$ μm. This is coherent with the shear band thickness of 1 μm measured below the fracture surface in previous work, increasing up to 3 μm in the presence of cavities [1].

The amplitude of the shear is given by the shear offset Δz measured on the fracture surface, i.e. the length on which the specimen was purely sheared. Indeed, fracture initiates and propagates by a through-thickness mode III shear, and ends by a mode II shear at its edges [2]. Some ripples were sometimes formed at the edge of the sheared surface in the fracture initiation zone and were not taken into account in the measurement of the sheared surface. Indeed, these ripples are formed during the dissipation of a large amount of plastic work on free surfaces before the crack propagation [2].

The plastic work dissipated by the through-thickness shear can be defined as the integral of the true shear stress τ and the true shear strain rate $\dot{\gamma}$ over the shearing time: $W_p = \int \tau(t)\dot{\gamma}(t)\partial t$ [J m^{-3}]. However, the evolution of the true shear stress and true shear strain rate are unknown. A reasonable assumption consists in considering the true shear stress and strain rate as constant. The true shear stress is estimated from the true tensile fracture stress, σ_f, and the average angle θ between the fracture surface and the tensile direction, for the Cu-coated tensile specimen: $\tau = \sigma_f . \sin\theta . \cos\theta \sim 700$ MPa. The shear strain rate is estimated from the shearing speed v_s and from the half-thickness of the shear band $\dot{\gamma} = \frac{v_s}{2h}$ [s^{-1}]. The plastic work rate is therefore estimated as $\dot{W}_p = \frac{\tau v_s}{2h}$ [J m^{-3} s^{-1}]. The shearing time Δt [s] is taken as the ratio between the shear offset Δz and the shearing speed v_s.

While the shearing speed v_s through the thickness of the tensile specimen could not be measured, the fracture speed, i.e. the speed of the crack propagation through the width of the tensile specimen v_p, was measured using high-speed imaging in a previous work [2]. Fig. 3 presents the variation of the average crack propagation speed with the normalized crack propagation distance. The fracture speed increases up to a maximum of 1840 m s^{-1} after 20–50% of the normalized crack propagation distance, then decreases to a crack stop after about 80% of this distance. The crack arrest corresponds to the transition between mode III and mode II crack propagation. The crack speed increases then up to 940 m s^{-1} until the end of the crack propagation. As the crack speed evolution follows the same trend for all recorded crack propagations, an average evolution of the crack propagation speed was obtained by averaging three interpolation curves. According to Miracle *et al.* [29], the shearing speed is related to the crack propagation speed by the following relation: $v_s = 4\gamma v_p \sim 0.08 v_p$, where γ is the elastic shear strain, given by the shearing stress τ divided by the shear modulus G (around 35 GPa for a β -metastable Ti alloy [35]). The maximum measured fracture speed was 1840 m s^{-1} [2], therefore the shearing speed in Ti12Mo can increase up to about 150 m s^{-1}. The shearing speed will thus be varied between 0 and 150 m s^{-1} in the different models.

Finally, the Taylor-Quinney coefficient β defines the heat rate as a proportion of the plastic work rate externally applied. It is generally taken as 0.9 [15–17,31], even though this coefficient varies with many parameters (loading conditions, temperature, material, grain size, ...) as it depends on the fraction of applied plastic work rate stored inside the microstructure [36]. This coefficient may also vary with the strain level [37]. A large variability of the Taylor-Quinney coefficient exists therefore in the literature for the same material [36–38]. A Taylor-Quinney coefficient varying between 0.2 and 1 was estimated in TA6V alloy [38,39] and between 0.75 and 1 in Cp-Ti alloy [38]. A significant increase of the coefficient was measured in Cp-Ti when the loading conditions favor mechanical twinning, as the formation of twins seems less effective to store internal energy as compared to dislocation glide [38]. Moreover, Kositski *et al.* [37], using molecular dynamics simulations, showed that a coefficient close to 1 can be obtained at large strain levels when the density of stored defects within the microstructure reaches a steady state level. A coefficient larger than 1 could even be momentarily reached with the activation of mechanisms decreasing the internal energy of the microstructure, as grain growth for example [37]. Therefore, a large Taylor-Quinney coefficient can be expected at the end of the deformation of Ti-12Mo, considering the large dislocations density already stored and the dynamic recrystallization probably activated during adiabatic shear banding [1]. In the absence of actual measurement of this coefficient, a relatively large value of 0.9 is considered.

Table 2
Parameters of the models. ρ, C_p, α are the density, heat capacity and thermal diffusivity at 1118.5 K of Ti-12Mo, respectively. h is the half-thickness of the shear band; Δz is the length of the shear offset created during the through-thickness shear; τ is true shear stress; v_s is the shearing speed; β is the Taylor-Quinney coefficient defining the proportion of work converted into heat.

ρ [kg m^{-3}]	C_p [J kg^{-1} K^{-1}]	α [m^2 s^{-1}]	h [m]	Δz [m]	τ [Pa]	v_s [m s^{-1}]	β [/]
4690	695	6.97 10^{-6}	5 10^{-7}	27 10^{-6}	7 10^8	0 – 150	0.9

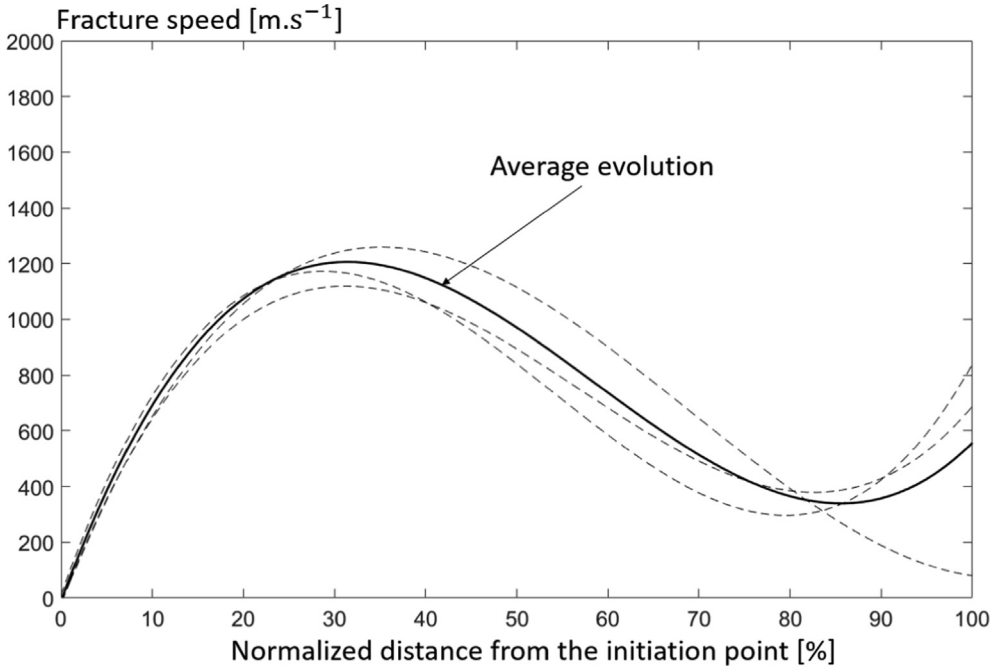

Fig. 3. Average evolution of the fracture speed in Ti-12Mo as a function of the normalized distance from the fracture initiation point to the end of the crack propagation, estimated from three high-speed imaging measurements (dotted lines) at the end of quasi-static tensile presented in a previous work [2].

4.4. One-dimensional models

The first model presented in this paper describing the temperature rise produced during shear banding was proposed by Lewandowski and Greer [26] when they assessed the fusible coating method. In their work, the temperature rise ΔT_1 was estimated from the one-dimensional diffusion equation applied to thin films, in which the heat H [J m^{-2}] is produced instantaneously and homogeneously along a zero-thickness shear band:

$$\Delta T_1 = \frac{H}{2\rho C_p}\sqrt{\frac{1}{\pi\alpha t}}e^{-\frac{x^2}{4\alpha t}}; \tag{1}$$

with x [m] is the distance from the shear band and t [s] is the time following the release of the heat content of the shear band. The maximum temperature $\Delta T_{1,m}$ reached at a distance x from the shear band is given by:

$$\Delta T_{1,m} = \frac{H}{\rho C_p}\frac{1}{x\sqrt{2\pi e}} \tag{2}$$

Following the work of Lewandowski *et al.* [26], the heat content can be estimated from the distance over which Cu and Pd coatings melted. The estimations are very close, 11.5 kJ m^{-2} for the Cu coating and 12.4 kJ m^{-2} for the Pd coating. A mean heat content of 12.0 kJ m^{-2} will then be used. As this model considers an instantaneous heat production in a zero-thickness band, the temperature tends to infinite in the shear band when the heat is produced. To estimate the maximum temperature reached in the shear band $\Delta T_{1,\mathrm{m}}^{x=0}$, a shearing time Δt must be introduced:

$$\Delta T_{1,\mathrm{m}}^{x=0} = \frac{H}{\rho C_p}\sqrt{\frac{1}{\pi\alpha\Delta t}} \tag{3}$$

Fig. 4(a) presents the variation of the maximum temperature reached as a function of the distance from the shear band according to this simple model based on one-dimensional heat diffusion. Equation (2) was bounded by Equation (3) for the maximum temperature reached to avoid the non-physical divergent temperature predicted by Equation (2) when approaching the shear band. The maximum shearing speed induces a temperature of 2147 K in the shear band, i.e. over the melting temperature of Ti-12Mo (1973 K). Minimum shearing speeds of 50 m s^{-1} and 103 m s^{-1} are required to reach the melting temperatures of the Cu and Pd coatings, respectively. Obviously, the model fits well with the length of melted Cu and Pd coatings. The temperature is overestimated regarding the Al coating, as expected (see Section 4.2), but is also underestimated regarding the Sn and Zn coatings. Moreover, the transition between Equations (2) and (3) is physically incorrect.

A second model was proposed by Wang *et al.* [31], for which the temperature rise ΔT_2 was still estimated from a one-dimensional diffusion equation but for which the heat is produced homogeneously in a shear band of finite thickness, during a non-zero shearing time. The heat diffusion equation is divided in two parts during shearing, corresponding to the material inside and outside of the shear band:

$$\frac{\partial \Delta T_2}{\partial t} = \alpha\frac{\partial^2 \Delta T_2}{\partial x^2} + \frac{\dot{\omega}}{\rho C_p} \quad \text{for } x < h, 0 < t < \Delta t \tag{4a}$$

$$\frac{\partial \Delta T_2}{\partial t} = \alpha\frac{\partial^2 \Delta T_2}{\partial x^2} \quad \text{for } x > h, 0 < t < \Delta t \tag{4b}$$

where $T_2(x,t)$ is the variation of the temperature with the distance x from the center of the shear band and the time t; and $\dot{\omega}$ is the heat release rate estimated from the dissipated plastic work rate [J m^{-3} s^{-1}].

The resolution of Eqs. (4a) and (4b) for a zero initial temperature gives [40]:

$$\Delta T_2 = \frac{\dot{\omega} t}{\rho C_p}\left[1 - 2i^2 erfc\left(\frac{h-x}{2\sqrt{\alpha t}}\right) - 2i^2 erfc\left(\frac{h+x}{2\sqrt{\alpha t}}\right)\right] \quad \text{for } x < h,\ 0 < t < \Delta t \tag{5a}$$

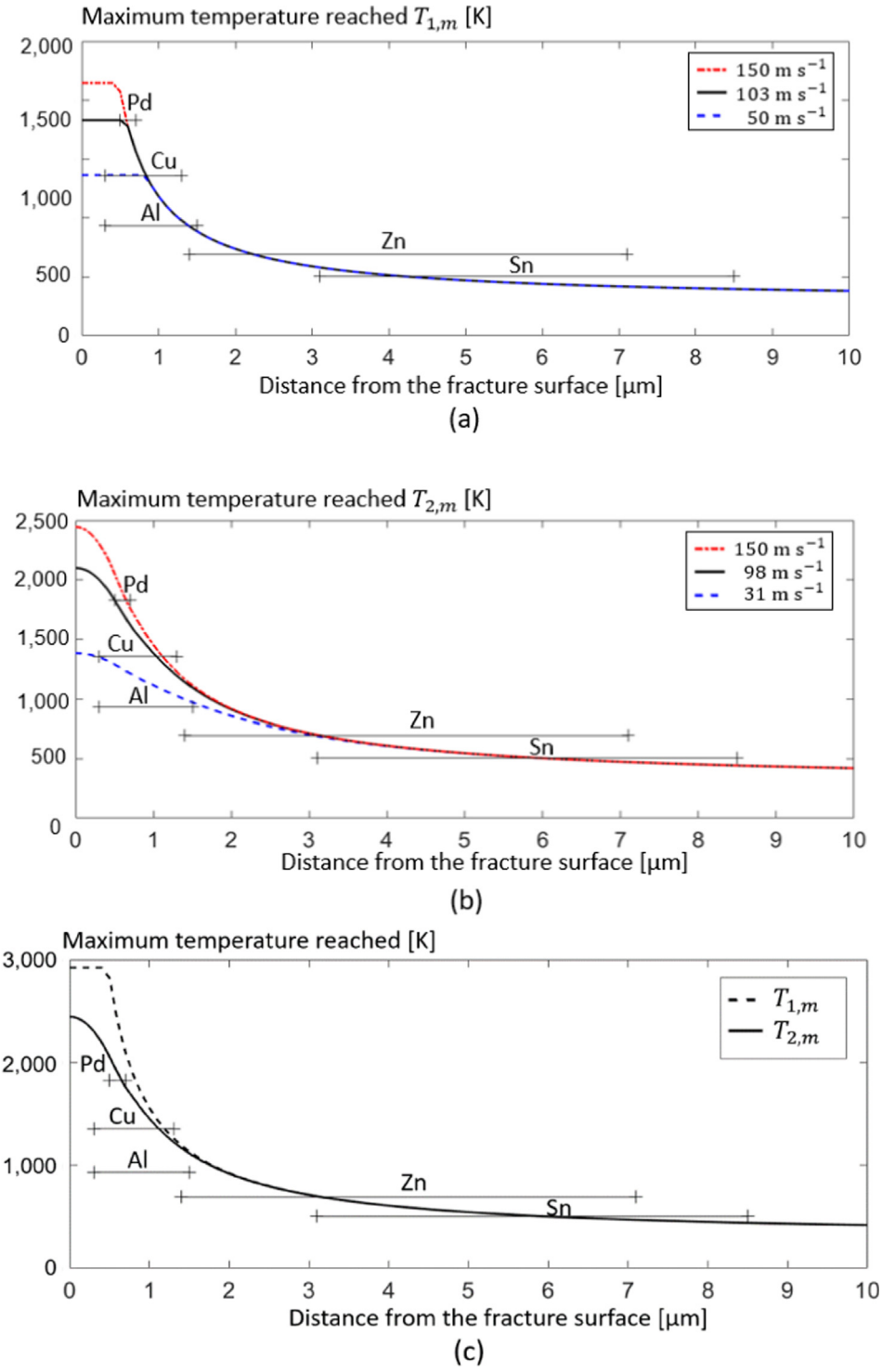

Fig. 4. Maximum temperature reached at a given distance from the center of the shear band, considering the heat produced (a) instantaneously and in a zero-thickness plane [26]; (b) during the shearing time in a shear band of finite thickness [31]. (c) Comparison between the first model ($T_{1,m}$) and the second model ($T_{2,m}$) for the heat content estimated from the mechanical work, and a shearing speed of 150 m s^{-1}.

$$\Delta T_2 = \frac{\dot{\omega} t}{\rho C_p}\left[2i^2erfc\left(\frac{x-h}{2\sqrt{\alpha t}}\right) - 2i^2erfc\left(\frac{h+x}{2\sqrt{\alpha t}}\right)\right] \quad \text{for} \quad x > h,\ 0 < t < \Delta t \tag{5b}$$

where $i^2erfc(x) = 0.25\left[(1+2x^2)erfc(x) - \frac{2}{\sqrt{\pi}}x\exp(-x^2)\right]$.

For $t > \Delta t$, Eq. (4b) can be resolved with an initial distribution of temperature $f(x)$ corresponding to the distribution of temperature at the end of the shear [41]:

$$\Delta T_2 = \frac{1}{\sqrt{4\pi\alpha t'}}\int f(u)\exp\left(-\frac{(x-u)^2}{4\alpha t'}\right)du \quad \text{for} \quad t' > 0,\ t = t' + \Delta t \tag{6}$$

Fig. 4(b) presents the variation of the maximum temperature reached as a function of the distance from the shear band according to this more detailed analytical model of one-dimensional heat diffusion. As for the first model, the shearing speed mostly influences the temperature rise in and near the shear band. The curves are superimposed at a larger distance from the fracture surface as they all correspond to the same heat content. Shearing speeds ranging from 31 m s^{-1} to 150 m s^{-1} seem adequate to fit with the melted lengths of Cu coating. It ranges from 98 m s^{-1} to 150 m s^{-1} for the Pd coating. The melted lengths of Al coating are underestimated, as expected, but the temperature distribution quite correctly fits with the melted lengths of Sn and Zn coatings.

In order to compare the first and second models, the same heat content must be used. The total heat content H [J m^{-2}] dissipated during shear banding can be estimated from the heat release rate as:

$$H = 2h\beta\dot{\omega}\Delta t, \tag{7}$$

which can be simplified considering the definition of the heat release rate $\dot{\omega}$ [J m^{-3} s^{-1}] given in Section 4.3:

$$H = \beta\tau\Delta z. \tag{8}$$

In the case of shear banding in Ti-12Mo, the heat content was estimated as 17.0 kJ m^{-2}.

The maximum temperature distribution for the first and second models are represented in Fig. 4(c) for a shearing speed of 150 m s^{-1}. Without taking into account the thickness of the shear band, the first model with instantaneous release of heat in a zero-thickness band predicts a much higher temperature for distances smaller than 1 μm from the center of the shear band, i.e. over twice the thickness of the shear band. The distance over which the two models predict different temperatures increases when the shearing speed decreases, reaching up to 3 μm for a shearing speed of 31 m s^{-1} (Fig. 4(b)). As a consequence, the first model would lead to an underestimation of the heat content if the length of the melted coating is located in this zone, i.e. if the length of the melted coating is small. However, it was discussed in Section 4.2 that a small melted length is generally preferred to avoid zones of partially melted coatings and larger standard deviations of the measurements. A coating with a low melting temperature is therefore preferred when using the first model, while a coating with a higher melting temperature is preferred when using the second model.

As a conclusion, the first model is simpler and accurate enough to predict the correct order of magnitude of the temperature during shear banding. However, the thickness and shearing time must be taken into account if more accurate heat content and maximum temperature reached in and near the center of the shear band are required.

4.5. Two-dimensional model

Both models developed in the previous section consider the homogeneous release of heat in the shear band, in the whole section of the tensile specimen. However, fracture by shear banding is not a homogeneous process. Indeed, shear band first nucleates and then propagates. As a consequence, the temperature increases in two directions: along the thickness during the shearing step and along the width during the crack propagation [2]. We propose here a true two-dimensional heat diffusion model, based on multiple heat sources spread along the width of the tensile specimen, activated by the crack propagation and thus during the through-thickness shearing step. The time at which shear banding starts, t_i, and shear banding ends, t_f, are therefore different for each location along the width of the tensile specimen. Two-dimensional heat diffusion equations were used, based on the same structure as Eqs. 4(a) and 4(b), i.e. considering the heat diffusion inside ($x < h$) and outside ($x > h$) of the shear band all along the width of the tensile specimen:

$$\frac{\partial\Delta T_2}{\partial t} = \alpha\left(\frac{\partial^2\Delta T_2}{\partial x^2} + \frac{\partial^2\Delta T_2}{\partial y^2}\right) + \frac{\dot{\omega}}{\rho C_p} \quad \text{for} \quad x < h,\ t_i < t < t_f \tag{9a}$$

$$\frac{\partial\Delta T_2}{\partial t} = \alpha\left(\frac{\partial^2\Delta T_2}{\partial x^2} + \frac{\partial^2\Delta T_2}{\partial y^2}\right) \quad \text{for} \quad x > h,\ t_i < t < t_f \tag{9b}$$

with the heat release rate, $\dot{\omega} = \beta\tau\frac{v_s}{2h}$ [J m^{-3} s^{-1}]. To simplify the problem, the true shear stress τ and the thickness of the shear band $2h$ are considered constant during the crack propagation. The heat release rate therefore only varies with the shearing speed v_s. For the simulation, the shear offset Δz [m] and the shearing speed v_s [m s^{-1}] were estimated at several spots along the crack propagation path where the length of melted Cu coating was measured, every 90 μm on average. The time at which shear banding starts at each measurement spot $t_i = \int\frac{\partial y}{v_p(y)}$ is given by the time after fracture initiation at which the crack reaches the given measurement spot at the fracture speed v_p. The time at which shear banding ends $t_f = t_i + \Delta t$ is given by the total shearing time Δt at the given measurement spot, computed from the ratio between the local width of sheared offset Δz and the local value of the shearing speed v_s. The heat content brought in each measurement spot depends therefore mainly on the width of the local shear offset Δz, while the heat rate depends on the local shearing speed v_s.

The model relies on the variation of the shearing speed during the crack propagation. Fig. 5 presents the estimated evolution of this shearing speed, based on the average evolution of the crack propagation speed during the mode III crack propagation. Close to the end of the fracture process, the crack propagation switches to mode II shear fracture. In these zones, the Cu coating was removed near the fracture surface, hence the edges of the specimen could not be mapped. Only the speed variation for the first 80% of the crack propagation distance when the crack propagates in mode III was thus used for the evolution of the shearing speed in the simulation.

Eqs. (9a) and (9b) were solved by the finite elements method using COMSOL Multiphysics software. The length of the sample was fixed to 500 μm to limit the size of the mesh. The boundary conditions were defined as:

- Plane symmetry on either side of the center of the shear band;
- Adiabatic conditions for the lateral sides of the sample;
- Fixed temperature of 293 K at the extremity of the tensile sample far from the fracture surface.

The complete evolutions of the physical properties ρ, c_p, α with temperature were interpolated by cubic splines of the measured data (presented in Supplementary Figs. 1, 2 and 3) up to the maximum temperature at which they were measured (at 1260 K for the heat capacity c_p and at 1574 K for the heat diffusivity α). In order to estimate the evolution of the physical properties outside of the measured temperature range, the values were extrapolated according to a simple expected temperature evolution (linear evolution for the heat capacity and the density, quadratic evolution for the thermal diffusivity) [42].

The validity of the simulation as well as the quality of the mesh refinement were checked by comparing this third model (considering temperature independent materials properties and a constant shearing speed) with the second one-dimensional model presented

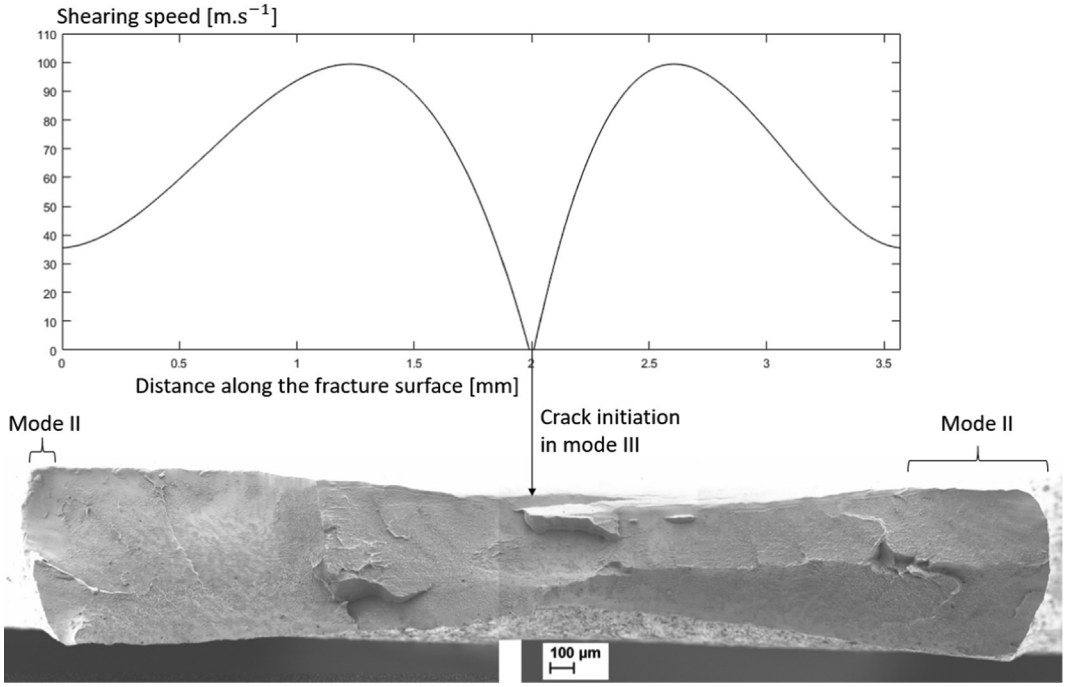

Fig. 5. Evolution of the shearing speed for the Cu coated tensile specimen, estimated based on the average crack propagation speed during the first 80% of the crack propagation from Fig. 3 for each point where the length of melted Cu coating was measured. The associated fracture surface is presented with the crack initiation site, and the two edges fractured in mode II not taken into account in the simulation.

in Section 4.4. Similar temperature variations were obtained with both models (Supplementary Fig. 4).

Fig. 6(a) presents the variation of the maximum temperature reached with the distance from the shear band during the propagation of the crack. The temperature in the center of the shear band remains close to room temperature at fracture initiation and increases up to the melting temperature of the alloy during its propagation. Temperatures larger than the ones predicted in the one-dimensional heat diffusion simulation of the second model are locally obtained, mainly because of the locally larger shear offset Δz, implying a larger heat content. It is worth noting that the three models presented in Sections 4.4 and 4.5 do not take into account the energies associated to the various transformations occurring during heating, i.e. reverse martensite transformation into β, dynamic recrystallization and local melting.

The prediction fits quite well with the variations of the measured Cu melted coating. Moreover, the zones where the melting temperature of the alloy was reached also correspond to the zones where large Taylor patterns were observed on the fracture surface (from 0 to 1.1 mm along the fracture surface in Figs. 5, 6(a)). Finally, Fig. 6(b) compares the average measured length of the melted coatings with the average distance at which the associated melting temperature was simulated. The latter fits very well with the measured data (except for the Al coating as discussed in Section 4.2).

A two-dimensional approach is needed to model accurately the temperature evolution during the propagation of a shear band. The maximum temperature reached at the center of the shear band increases during its propagation, contrarily to what Miracle *et al.* proposed [29]. Moreover, the fracture speed is not constant during the propagation of the crack in the case of the unstable fracture of Ti-12Mo, contrarily to what is usually modeled in the literature for adiabatic shear banding [25,33]. The shearing speed and shearing time are not constant during the propagation of the shear band, resulting in waves of larger temperature rise during its propagation.

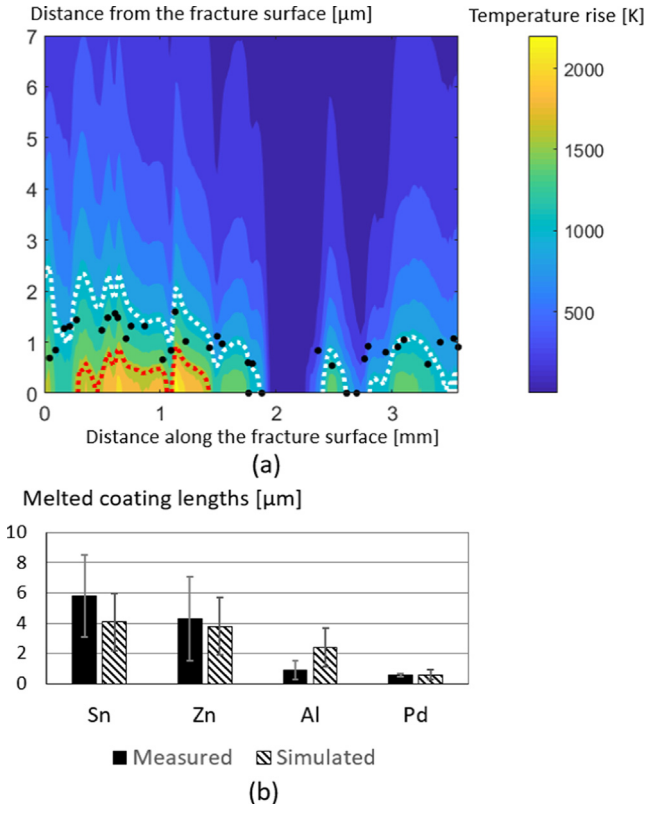

Fig. 6. (a) Simulated 2D map of the maximum temperature reached in the case of the Cu coated tensile specimen. The black dots correspond to the actual measurements of the length of melted Cu coatings. The red and white dotted lines correspond to the isothermal lines predicted by the model at 1953 K (ΔT_m^{Ti12Mo}) and at 1338 K (ΔT_m^{Cu}), respectively. (b) Comparison of the measured and simulated lengths over which melting occurred for the different coatings.

4.6. Estimation of the temperature rise for other materials

Based on the present analysis carried out in the case of the Ti-12Mo alloy, the question of the maximum temperature that can be reached for other materials exhibiting the same fracture mechanism can be raised. More generally, what could be the maximum temperature rise during unstable adiabatic shear banding, for example in shear lips at the end of the fracture of a ductile crystalline alloy or during fracture of bulk metallic glasses?

The evolution of the temperature rise predicted for Ti-12Mo is quite accurate because most of the parameters dictating this shear banding were directly measured from the fractured tensile specimen. In order to predict the temperature rise in a material without having access to the broken samples, the different parameters of the shear localization must be estimated from the properties of the materials.

The heat capacity C_p and thermal diffusivity α are fixed at about half their melting temperature, as it gave a quite accurate temperature distribution for Ti-12Mo compared to the temperature distribution obtained by varying the physical properties with temperature.

As for the previous models, the shear stress is kept constant and estimated from the true tensile fracture stress, σ_f, and the fracture angle, θ, taken as 45°, which corresponds to a pure shear fracture. The true tensile fracture stress σ_f can itself be easily obtained from the nominal stress at fracture σ_{nf} and the reduction of area RA:

$$\tau = \sigma_f . \sin\theta . \cos\theta \sim \frac{1}{2}\frac{\sigma_{nf}}{1-\frac{RA}{100}}; \tag{10}$$

The maximum shearing speed v_s is estimated from the speed of a shear wave c_t in the material, its shear stress τ and its shear modulus G. The maximum shear propagation speed v_p has been estimated at about 60% of the speed of a shear wave c_t in the material during unstable shear propagation [16,33,43], which is coherent with the crack propagation speed measured in Ti-12Mo ($v_p = 59\%\, c_t$). The shearing speed is itself bounded by the shear propagation speed through the elastic shear strain γ, as developed by Miracle *et al.* [29]:

$$v_s = 4\gamma v_p \sim \frac{2\tau}{G} c_t \tag{11}$$

The shear offset Δz is required to estimate the total shearing time:

$$\Delta t = \frac{\Delta z}{v_s}; \tag{12}$$

As a first approximation, the same shear offset as measured for Ti-12Mo will be used here. However, the shear offset probably varies with many parameters, i.e. the mechanical properties of the material, the type of loading or the local triaxiality at fracture. For example, Lewandowski *et al.* [26] measured a shear offset of the order of 1 μm after a banding test in a bulk metallic glass. Miracle *et al.* [29] also proposed that the shear offset varies with the square of the dimension of the specimen. A post-fracture measurement is advised to estimate more accurately this important parameter.

The thickness of the shear band in which the plastic work localizes also influences the estimation of the temperature rise. Indeed, it was shown in Section 4.4 that considering a zero-thickness shear band leads to an overestimation of the local temperature rise. Dodd and Bai [44] derived an estimation of the thickness of an adiabatic shear band, which predicts the correct order of magnitude of the thickness of adiabatic shear bands measured experimentally [19,22]:

$$h \sim \sqrt{\frac{\lambda T}{\tau \dot{\gamma}}} \tag{13}$$

where λ is the thermal conductivity [$W\, m^{-1}\, K^{-1}$], and $T, \tau, \dot{\gamma}$ are the local temperature, shear stress and shear strain rate in the shear band. The thickness of the shear band can also be linked to the shear strain rate with the shearing speed:

$$h = \frac{v_s}{2\dot{\gamma}} \tag{14}$$

Combining Eqs. (13) and (14), an estimation of the half-thickness independent from the local shear strain is obtained:

$$h \sim \frac{2\lambda T}{\tau v_s} \tag{15}$$

Hence, the order of magnitude of the local temperature is needed for the estimation of the thickness of the shear band. While overestimating the local temperature rise, the zero-thickness estimation of the maximum temperature rise in the shear band (Eq. (3)) predicts the correct order of magnitude (as discussed in Section 4.4). An upper bound set by the melting temperature of the alloy was applied.

The Taylor-Quinney coefficient varies as a function of the material but also of the initial microstructure, loading conditions, applied strain rate and strain level, as discussed in Section 4.3. As this model aims at giving a general estimation of the local temperature rise brought by an unstable fracture in different materials, a constant Taylor-Quinney coefficient of 0.9 is considered.

Table 3 summarizes the parameters used for different materials considered as hypothetically bringing shear banding.

A thickness of 1.9 μm, 1.4 μm, 3 μm, 13.9 μm and 0.3 μm are predicted for Ti-12Mo, Ti-6Al-4V, 316L stainless steel, pure Al and Vitreloy 1, respectively. The predicted thickness of the shear band in Ti-12Mo fits well with the 1–3 μm range of shear band thickness measured on fractured tensile specimen [1]. Thicknesses from 1 μm to 40 μm were observed for Ti-6Al-4V alloy [45,46] and from 10 μm to 16 μm for 316L stainless steel [47]. The smaller estimated band thickness compared to the measured ones might come from a larger estimated shear speed, taken as the theoretical maximum shear speed in the material (Eq. (15)). In the case of bulk metallic glasses as Vitreloy 1, the predicted shear band thickness is not very far from the measured thicknesses, in the range of 10 nm to

Table 3
Parameters of the models. ρ, C_p, α are the density, heat capacity and thermal diffusivity taken at half their melting temperature in the amorphous state for Vitreloy 1; ΔT_m is the temperature rise to the liquidus; Δz is the length of the shear offset, taken as the one measured on Ti-12Mo except for BMG where the shear offset was measured by Lewandoswki *et al* [26]; τ is the true shear stress; G is the shear modulus and c_t is the speed of an elastic shear wave propagating in the material.

	ρ [$kg\, m^{-3}$]	C_p [$J\, kg^{-1}\, K^{-1}$]	α [$cm^2\, s^{-1}$]	ΔT_m [K]	Δz [μm]	τ [MPa]	G [GPa]	c_t [$m\, s^{-1}$]
Ti-12Mo	4688	702	7.4	1680	27	700	35	3125
Ti-6Al-4V	4254	710	5.34	1630	27	690	40	3125
316L stainless steel	7521	603	5.4	1357	27	660	77.2	3100
Pure Al	2588	908	97.9	640	27	250	27	3040
Vitreloy 1	5991	620	3.5	644	1.5	850	32	2470

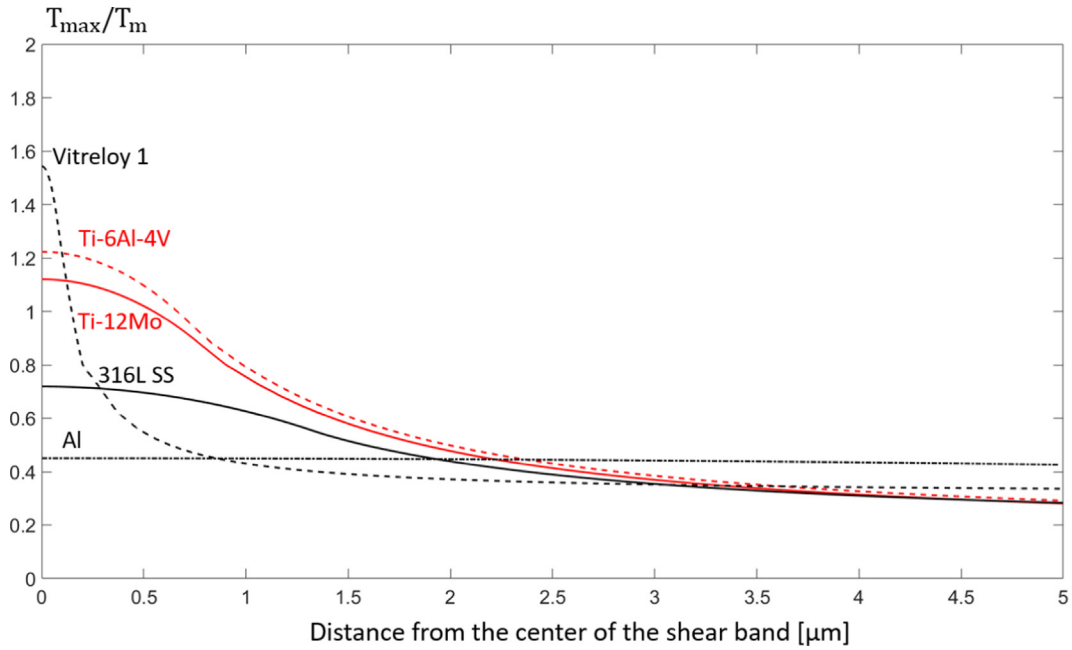

Fig. 7. Maximum temperature reached normalized by their melting temperature for Ti-6Al-4V, Ti-12Mo, Vitreloy 1, 316L stainless steel and pure Al, computed from Equations (10), (11), (12), (13) and (15) and the parameters given in Table 3.

100 nm [48,49]. A shear band thickness of 90 nm, in the range of the measured thicknesses, is predicted with our model, considering the glass transition temperature T_g as the upper bound instead of considering the melting temperature.

Fig. 7 presents the maximum temperature T_{max} estimated for the various alloys listed in Table 3, normalized by their respective melting temperature T_m. A temperature increasing up to the melting temperature is predicted for Ti-12Mo, Ti-6Al-4V and in the bulk metallic glass Vitreloy 1, in agreement with the observation of melted features on the fracture surface of the respective alloys [1,10,50]. A significant temperature rise close to the melting temperature is also predicted for 316L stainless steel. On the other hand, the temperature rise is limited in materials with large thermal conductivity such as aluminum.

While direct measurements as high-speed imaging of the crack propagation and fractography allow a more accurate estimation of the parameters such as the shearing speed, the shearing time and the shear band thickness, the analytical equations derived in this section bring a quite accurate first approximation. Non-negligible temperature rise can be expected in most alloys during unstable shear deformation, except in alloys presenting a very large thermal conductivity such as Al alloys.

5. Conclusion

The fusible coating method was used to estimate the local temperature rise occurring during unstable fracture of the TRIP-TWIP β -metastable Ti-12Mo alloy. 5 different coatings were used to measure the variation of the distance over which their respective melting temperatures were reached. The most appropriate coatings regarding the estimated temperature rise were then considered for modelling the thermal history accompanying crack propagation. Two one-dimensional heat diffusion equations were compared, highlighting the importance of shearing time and shear band thickness for the prediction of temperature rise during adiabatic shear banding.

To the best authors' knowledge, a two-dimensional simulation of the temperature rise accompanying unstable shear band propagation was combined for the first time with an experimental estimation with the fusible coating method. This temperature rise is not constant and evolve with the shearing speed.

An estimation of the local true shear stress, shearing speed, shearing time and shear band thickness was finally calculated from classical mechanical/physical properties in order to predict the order of magnitude of temperature rise during similar unstable shearing in different alloys (Ti alloys, 316L stainless steel, pure Al and bulk metallic glass Vitreloy 1) from easily accessible data. Except for alloys with very large thermal conductivity as pure Al, non-negligible temperature rise can be expected in most alloys during unstable shear deformation. Based on this conclusion, it would worth assessing the occurrence of local melting during fracture of several advanced alloys such as stainless or TWIP steels.

Complete finite element simulations would allow more accurate prediction of the local stresses and temperature evolution during the shear band propagation. However, it would require the complete data set of the mechanical and physical properties including thermomechanical coupling, with large computation costs. The analytical models proposed here are much simpler and allow a better prediction of the temperature rise than the usually used 1D diffusion equation for thin films.

CRediT authorship contribution statement

L. Choisez: Methodology, Investigation, Formal analysis, Writing – original draft. **G. Roy:** Software, Validation, Writing – review & editing. **P.J. Jacques:** Conceptualization, Supervision, Writing – review & editing.

Declaration of Competing Interest

The authors declare that they have no known competing financial interests or personal relationships that could have appeared to influence the work reported in this paper.

Acknowledgments

The Fonds National de Recherche Scientifique FNRS is gratefully acknowledged for the grant n°T.0127.19 and the research grant of L.C. The authors are thankful to O. Poncelet for the deposition of the different coatings, to J.-P. Erauw for the measurement of the thermal properties of the alloy and to P. Verleysen for the fruitful discussions.

Data availability

The datasets generated during and/or analyzed during the current study are available from the corresponding author on reasonable request.

Appendix A. Supplementary material

Supplementary data to this article can be found online at https://doi.org/10.1016/j.matdes.2021.110269.

References

[1] L. Choisez, L. Ding, M. Marteleur, H. Idrissi, T. Pardoen, P.J. Jacques, High temperature rise dominated cracking mechanisms in ultra-ductile and tough titanium alloy, Nat. Commun. 11 (2020) 1–8, https://doi.org/10.1038/s41467-020-15772-1.
[2] L. Choisez, A. Elmahdy, P. Verleysen, P.J. Jacques, Fracture mechanisms in flat and cylindrical tensile specimens of TRIP-TWIP beta-metastable Ti-12Mo alloy, Acta Mater. 220 (2021), https://doi.org/10.1016/j.actamat.2021.117294 117294.
[3] S.D. Antolovich, R.W. Armstrong, Plastic strain localization in metals: origins and consequences, Prog. Mater. Sci. 59 (2014) 1–160, https://doi.org/10.1016/j.pmatsci.2013.06.001.
[4] Z.S. Basinski, The instability of plastic flow of metals at very low temperatures, Proc. R. Soc. London A Math. Phys. Eng. Sci. 240 (1957) 229–242, https://doi.org/10.1098/rspa.1957.0079.
[5] V.M. Segal, S. Ferrasse, F. Alford, Tensile testing of ultra fine grained metals, Mater. Sci. Eng. A. 422 (1-2) (2006) 321–326, https://doi.org/10.1016/j.msea.2006.02.016.
[6] A.L. Greer, Y.Q. Cheng, E. Ma, Shear bands in metallic glasses, Mater. Sci. Eng. R Reports. 74 (4) (2013) 71–132, https://doi.org/10.1016/j.mser.2013.04.001.
[7] M. Marteleur, F. Sun, T. Gloriant, P. Vermaut, P.J. Jacques, F. Prima, On the design of new β-metastable titanium alloys with improved work hardening rate thanks to simultaneous TRIP and TWIP effects, Scr. Mater. 66 (10) (2012) 749–752, https://doi.org/10.1016/j.scriptamat.2012.01.049.
[8] J.D. Bryant, D.D. Makel, H.G.F. Wilsdorf, Observations on the effect of temperature rise at fracture in two titanium alloys, Mater. Sci. Eng. 77 (1986) 85–93, https://doi.org/10.1016/0025-5416(86)90356-3.
[9] D.D. Makel, H.G.F. Wilsdorf, Localized melting at separation of AISI 4340 steel tensile samples, Mater. Sci. Eng. A. 142 (1) (1991) 107–114, https://doi.org/10.1016/0921-5093(91)90759-G.
[10] D.D. Makel, D. Eylon, The effect of microstructure on localized melting at separation in Ti-6Al-4V tensile samples, Metall. Trans. A Phys. Metall. Mater. Sci. 21 (1990) 3127–3136, https://doi.org/10.1007/BF02647309.
[11] T.W. Wright, Shear band susceptibility: Work hardening materials, Int. J. Plast. 8 (5) (1992) 583–602, https://doi.org/10.1016/0749-6419(92)90032-8.
[12] S. Braeck, Y.Y. Podladchikov, S. Medvedev, Spontaneous dissipation of elastic energy by self-localizing thermal runaway, Phys. Rev. E - Stat. Nonlinear, Soft Matter Phys. 80 (2009) 1–15, https://doi.org/10.1103/PhysRevE.80.046105.
[13] J. Lemonds, A. Needleman, Finite element analyses of shear localization in rate and temperature dependent solids, Mech. Mater. 5 (4) (1986) 339–361.
[14] R.C. Batra, C.H. Kim, Effect of thermal conductivity on the initiation, growth and bandwidth of adiabatic shear bands, Int. J. Eng. Sci. 29 (8) (1991) 949–960, https://doi.org/10.1016/0020-7225(91)90168-3.
[15] M. Zhou, A.J. Rosakis, G. Ravichandran, On the growth of shear bands and failure-mode transition in prenotched plates: a comparison of singly and doubly notched specimens, Int. J. Plast. 14 (4-5) (1998) 435–451, https://doi.org/10.1016/S0749-6419(98)00003-5.
[16] Shaofan Li, Wing Kam Liu, Ares J. Rosakis, Ted Belytschko, Wei Hao, Mesh-free Galerkin simulations of dynamic shear band propagation and failure mode transition, Int. J. Solids Struct. 39 (5) (2002) 1213–1240, https://doi.org/10.1016/S0020-7683(01)00188-3.
[17] S. Medyanik, W. Liu, S. Li, On criteria for dynamic adiabatic shear band propagation, J. Mech. Phys. Solids. 55 (7) (2007) 1439–1461, https://doi.org/10.1016/j.jmps.2006.12.006.
[18] Balbina Wcisło, Jerzy Pamin, Local and non-local thermomechanical modeling of elastic-plastic materials undergoing large strains, Int. J. Numer. Methods Eng. 109 (1) (2017) 102–124, https://doi.org/10.1002/nme.v109.110.1002/nme.5280.
[19] A. Marchand, J. Duffy, An experimental study of the formation process of adiabatic shear bands in a structural steel, J. Mech. Phys. Solids. 36 (3) (1988) 251–283.
[20] J. Duffy, Y.C. Chi, On the measurement of local strain and temperature during the formation of adiabatic shear bands, Mater. Sci. Eng. A. 157 (2) (1992) 195–210, https://doi.org/10.1016/0921-5093(92)90026-W.
[21] M. Zhou, G. Ravichandran, A.J. Rosakis, Dynamically propagating shear bands in impact-loaded prenotched plates - I. Experimental investigations of temperature signatures and propagation speed, J. Mech. Phys. Solids. 44 (1996) 981–1006, https://doi.org/10.1016/0022-5096(96)00004-X.
[22] Shih-chieh Liao, J. Duffy, Adiabatic shear bands in a TI-6Al-4V titanium alloy, J. Mech. Phys. Solids. 46 (11) (1998) 2201–2231, https://doi.org/10.1016/S0022-5096(98)00044-1.
[23] P.R. Guduru, A.J. Rosakis, G. Ravichandran, Dynamic shear bands: an investigation using high speed optical and infrared diagnostics, Mech. Mater. 33 (7) (2001) 371–402, https://doi.org/10.1016/S0167-6636(01)00051-5.
[24] R. Clos, U. Schreppel, P. Veit, Temperature, microstructure and mechanical response during shear-band formation in different metallic materials, J. Phys. IV, EDP Sci. (2003) 111–116, https://doi.org/10.1051/jp4.
[25] A.-S. Bonnet-Lebouvier, A. Molinari, P. Lipinski, Analysis of the dynamic propagation of adiabatic shear bands, Int. J. Solids Struct. 39 (16) (2002) 4249–4269, https://doi.org/10.1016/S0020-7683(02)00244-5.
[26] J.J. Lewandowski, A.L. Greer, Temperature rise at shear bands in metallic glasses, Nat. Mater. 5 (2006) 15–18, https://doi.org/10.1038/nmat1536.
[27] L. Battezzati, D. Baldissin, Quantitative evaluation of lengthscales for temperature rise in shear bands and for failure of metallic glasses, Scr. Mater. 59 (2) (2008) 223–226, https://doi.org/10.1016/j.scriptamat.2008.03.016.
[28] K. Georgarakis, M. Aljerf, Y. Li, A. Lemoulec, F. Charlot, A.R. Yavari, K. Chornokhvostenko, E. Tabachnikova, G.A. Evangelakis, D.B. Miracle, A.L. Greer, T. Zhang, Shear band melting and serrated flow in metallic glasses, Appl. Phys. Lett. 93 (2008) 2006–2009, https://doi.org/10.1063/1.2956666.
[29] D.B. Miracle, A. Concustell, Y. Zhang, A.R. Yavari, A.L. Greer, Shear bands in metallic glasses: Size effects on thermal profiles, Acta Mater. 59 (7) (2011) 2831–2840, https://doi.org/10.1016/j.actamat.2011.01.022.
[30] S.K. Slaughter, F. Kertis, E. Deda, X. Gu, W.J. Wright, T.C. Hufnagel, Shear bands in metallic glasses are not necessarily hot, APL Mater. 2 (2014), https://doi.org/10.1063/1.4895605.
[31] J.G. Wang, Y. Pan, S.X. Song, B.A. Sun, G. Wang, Q.J. Zhai, K.C. Chan, W.H. Wang, How hot is a shear band in a metallic glass?, Mater Sci. Eng. A. 651 (2016) 321–331, https://doi.org/10.1016/j.msea.2015.10.125.
[32] Wendelin J. Wright, Rachel R. Byer, Xiaojun Gu, High-speed imaging of a bulk metallic glass during uniaxial compression, Appl. Phys. Lett. 102 (24) (2013) 241920, https://doi.org/10.1063/1.481174410.1063/1.4811744.1.
[33] L.B. Freund, F.H. Wu, M. Toulios, Initiation and propagation of shear band in antiplane shear deformation, in, Proc. Considere Meml. Symp. (1985) 125–143.
[34] L.L. Wang, H.S. Bao, W.X. Lu, The dependence of adiabatic shear banding in strain-rate, strain and temperature, J. Phys. 49 (C3) (1988) 207–214.
[35] C. Brozek, F. Sun, P. Vermaut, Y. Millet, A. Lenain, D. Embury, P.J. Jacques, F. Prima, A β-titanium alloy with extra high strain-hardening rate: design and mechanical properties, Scr. Mater. 114 (2016) 60–64, https://doi.org/10.1016/j.scriptamat.2015.11.020.
[36] C.K.C. Lieou, C.A. Bronkhorst, Thermomechanical conversion in metals: dislocation plasticity model evaluation of the Taylor-Quinney coefficient, Acta Mater. 202 (2021) 170–180, https://doi.org/10.1016/j.actamat.2020.10.037.
[37] Roman Kositski, Dan Mordehai, Employing molecular dynamics to shed light on the microstructural origins of the Taylor-Quinney coefficient, Acta Mater. 205 (2021) 116511, https://doi.org/10.1016/j.actamat.2020.116511.
[38] D. Rittel, L.H. Zhang, S. Osovski, The dependence of the Taylor-Quinney coefficient on the dynamic loading mode, J. Mech. Phys. Solids. 107 (2017) 96–114, https://doi.org/10.1016/j.jmps.2017.06.016.
[39] J. Galán, P. Verleysen, J. Degrieck, Thermal effects during tensile deformation of Ti-6Al-4V at different strain rates, Strain. 49 (4) (2013) 354–365, https://doi.org/10.1111/str.v49.410.1111/str.12042.
[40] H.S. Carslaw, J.C. Jaeger, Conduction of Heat in Solids, second ed., Oxford at the Clarendon Press, 1959.
[41] A.V. Luikov, Analytical Heat Diffusion Theory, second ed., Elsevier, 1968. DOI: 10.1016/0016-0032(70)90211-5.
[42] C.S. Kim, Thermophysical Properties of Stainless Steels Master Thesis, Argonne Natl. Lab., 1975.
[43] M. Zhou, G. Ravichandran, A.J. Rosakis, Dynamically propagating shear bands in impact-loaded prenotched plates - II. Numerical simulations, J. Mech. Phys. Solids. 44 (6) (1996) 1007–1032.
[44] B. Dodd, Y. Bai, Width of adiabatic shear bands, Mater. Sci. Technol. (United Kingdom) 1 (1) (1985) 38–40, https://doi.org/10.1179/mst.1985.1.1.38.
[45] H.A. Grebe, H. Pak, M.A. Meyers, Adiabatic shear localization in titanium and Ti-6 Pct AI-4 Pct V alloy, Metall. Trans. A. 16 (1985) 761–775.
[46] Y. Me-Bar, D. Shechtman, On the adiabatic shear of Ti-6A1-4V ballistic targets, Mater. Sci. Eng. 58 (1983) 181–188, https://doi.org/10.1016/0025-5416(83)90044-7.
[47] Q. Xue, E.K. Cerreta, G.T. Gray, Microstructural characteristics of post-shear localization in cold-rolled 316L stainless steel, Acta Mater. 55 (2) (2007) 691–704, https://doi.org/10.1016/j.actamat.2006.09.001.

[48] S.V. Ketov, D.V. Louzguine-Luzgin, Localized shear deformation and softening of bulk metallic glass: stress or temperature driven?, Sci Rep. 3 (2013) 2798, https://doi.org/10.1038/srep02798.
[49] Y. Zhang, A.L. Greer, Thickness of shear bands in metallic glasses, Appl. Phys. Lett. 89 (2006), https://doi.org/10.1063/1.2336598.
[50] C.T. Liu, L. Heatherly, J.A. Horton, D.S. Easton, C.A. Carmichael, J.L. Wright, J.H. Schneibel, M.H. Yoo, C.H. Chen, A. Inoue, Test environments and mechanical properties of Zr-base bulk amorphous alloys, Metall. Mater. Trans. A. 29 (1998) 1811–1820, https://doi.org/10.1007/s11661-998-0004-6.